ELSEVIER

Biochimica et Biophysica Acta 1561 (2002) 159–170

BIOCHIMICA ET BIOPHYSICA ACTA
BBA

www.bba-direct.com

Conformational changes of colicin Ia channel-forming domain upon membrane binding: a solid-state NMR study

Daniel Huster [a,1], Xiaolan Yao [a], Karen Jakes [b], Mei Hong [a,*]

[a] *Department of Chemistry, Iowa State University, Ames, IA 50011, USA*

[b] *Department of Physiology and Biophysics, Albert Einstein College of Medicine, 1300 Morris Park Avenue, Bronx, NY 10461, USA*

Received 26 September 2001; received in revised form 11 December 2001; accepted 18 December 2001

Abstract

Channel-forming colicins are bactericidal proteins that spontaneously insert into hydrophobic lipid bilayers. We have used magic-angle spinning solid-state nuclear magnetic resonance spectroscopy to examine the conformational differences between the water-soluble and the membrane-bound states of colicin Ia channel domain, and to study the effect of bound colicin on lipid bilayer structure and dynamics. We detected ^{13}C and ^{15}N isotropic chemical shift differences between the two forms of the protein, which indicate structural changes of the protein due to membrane binding. The Val Cα signal, unambiguously assigned by double-quantum experiments, gave a 0.6 ppm downfield shift in the isotropic position and a 4 ppm reduction in the anisotropic chemical shift span after membrane binding. These suggest that the α-helices in the membrane-bound colicin adopt more ideal helical torsion angles as they spread onto the membrane. Colicin binding significantly reduced the lipid chain order, as manifested by ^{2}H quadrupolar couplings. These results are consistent with the model that colicin Ia channel domain forms an extended helical array at the membrane–water interface upon membrane binding.

Keywords: Membrane protein; Chemical shift change; α-Helix filter; Magic angle spinning nuclear magnetic resonance; Resonance assignment

1. Introduction

Channel-forming colicins are plasmid-encoded bacterial toxins that are initially secreted as soluble proteins but later spontaneously partition into the inner membrane of susceptible bacteria [1]. Upon insertion and voltage activation, they form monomeric, non-selective channels that destroy the membrane potential of the target cell [2]. Thus, the conformational changes preceding channel formation and accompanying membrane insertion are crucial to colicin function. Such conformational changes are quite common among bacterial toxins such as the diphtheria toxin [3].

The soluble states of the colicin channel-forming domains are highly helical according to several crystal structures [4–7]. For example, the 3-Å crystal structure of the soluble form of colicin Ia channel domain [4] shows a globule of ten α-helices: two helices (C8 and C9) are hydrophobic and are sequestered in the interior of the molecule, while the remaining eight helices are largely amphipathic [8] and reside on the surface of the protein.

* Corresponding author. Fax: +1-515-294-0105.
E-mail address: mhong@iastate.edu (M. Hong).
[1] Present address: Institute of Medical Physics and Biophysics, University of Leipzig, Liebigstrasse 27, 04103 Leipzig, Germany.

0005-2736/02/$ – see front matter
PII: S0005-2736(02)00340-1

Membrane binding of colicins is thought to be initiated by both electrostatic and hydrophobic interactions with negatively charged lipid bilayers [9]. This binding process triggers the colicin channel domain to refold to a conformation that has been postulated to resemble either an 'umbrella' or a 'penknife' [10]. These models differ in the orientation of a hydrophobic helical hairpin formed by C8 and C9 in the bilayer, but both support the view that most residues are located at the membrane–water interface [11–14]. Moreover, a common implication of these structural models is that membrane binding causes large changes in the tertiary structure, but little or no change in the secondary structure of colicin channel domains.

A number of studies have been conducted to address the secondary structures of membrane-bound colicins, but gave ambiguous results. Fourier transform infrared experiments of colicins A, E1, and Ia reported that membrane binding caused the α-helical content to increase by 5–10% [15], by 30% [16], to remain constant [17,18], and even to decrease [19]. Far-UV circular dichroism (CD) experiments gave similarly divergent results on the helical content, ranging from a 25% increase [16] to being unperturbed [17,20]. These discrepancies may in part result from different lipid compositions and pH used in these experiments, and in part from different helical contents in the soluble state of the various colicins [2]. For colicin Ia, CD experiments detected little secondary structure change within the pH range 7.3–3.1. Only by a combination of a hydrophobic solvent (detergent octyl-β-D-glucopyranoside) and a strongly acidic pH was a small secondary structure alteration observed in the CD spectra [17]. On the other hand, evidence for tertiary structure changes was obtained from tryptophan fluorescence spectra of colicin Ia in the detergent.

To further elucidate the mechanism of the remarkable conformational rearrangement of colicins associated with the spontaneous membrane insertion, we carried out a solid-state nuclear magnetic resonance (NMR) study of the colicin Ia channel-forming domain (residues 453–626) in both the soluble and membrane-bound forms. Moreover, we investigated the effects of colicin Ia binding on the structure and dynamics of the lipid bilayer. Solid-state NMR has the advantage that relatively few constraints on membrane–protein sample preparation apply. This allows for the investigation of membrane proteins reconstituted into synthetic phospholipid bilayers, which simulate the biological membrane better than detergents. Moreover, solid-state NMR can probe the molecular structure and dynamics of membrane proteins directly without bulky extrinsic probes, thus minimizing perturbation to the native conformation of the proteins [21–23].

In this paper, we present the measurement of isotropic and anisotropic ^{13}C chemical shifts to characterize the structural differences between the soluble state and the membrane-bound closed-channel state of colicin Ia channel-forming domain. We also use ^{2}H and ^{31}P NMR to probe the lipid structure and dynamics in the presence of colicin Ia channel domain. Since we previously detected a substantial mobility increase of colicin Ia upon membrane binding [24], low-temperature experiments were conducted on the membrane protein sample to freeze out motions. This study was conducted on selectively and extensively ^{13}C-labeled protein samples, which provide multiple ^{13}C-labeled sites in each molecule. While the spectra do not have complete site resolution to yield atomic-level structural information, the multiple isotopic labels have the advantage of providing a global view of the effect of membrane binding on colicin structure.

2. Material and methods

1-Palmitoyl-d_{31}-2-oleoyl-*sn*-glycero-3-phosphocholine (POPC-d_{31}) and 1-palmitoyl-2-oleoyl-*sn*-glycero-3-phosphoglycerol (POPG) were purchased from Avanti Polar Lipids (Alabaster, AL) and used without further purification. Colicin Ia channel-forming domain was labeled selectively and extensively in ^{13}C and uniformly in ^{15}N following the TEASE (ten amino acid selective and extensive labeling) labeling protocol [25]. $^{15}NH_4Cl$, ^{15}N-Glu and [2-^{13}C]glycerol were purchased from Cambridge Isotope Laboratories (Andover, MA). Unlabeled amino acids were purchased from Sigma (St. Louis, MO).

2.1. Protein expression

Colicin Ia channel domain with an amino-terminal

His_6 tag, whose amino acid sequence is shown in Fig. 1a, was expressed from pKSJ120-containing *Escherichia coli* BL21(DE3). Cells were grown overnight at 37°C in 100 ml of a modified M9 medium containing, per liter, 1 g NH_4Cl, 4 g glycerol, 3 g KH_2PO_4, 6 g Na_2HPO_4, 0.5 g NaCl, 15 mg $CaCl_2$, 1 mM $MgSO_4$, the unlabeled amino acids Asp, Asn, Arg, Gln, Ile, Lys, Met, Pro, Thr and Glu at 150 μg/ml each, and 100 μg/ml ampicillin. The cells were pelleted and resuspended in 10 ml of the same medium, but containing 1.5 g $^{15}NH_4Cl$, 4 g [2-^{13}C]glycerol, and 150 μg/ml ^{15}N-Glu instead of unlabeled Glu. Those cells were used to inoculate 1 l of the stable-isotope-containing medium. The culture was grown at 37°C to $OD_{660} = 0.4$ and then induced with 1 mM isopropyl β-D-thiogalactopyranoside (IPTG). Cells were harvested after 3 h of induction at 37°C. The soluble His-tagged colicin Ia channel domain was purified on His-Bind metal chelation resin (Novagen, Madison, WI) as specified in the Novagen pET System Manual, except that the wash step was performed at 40 mM imidazole. The yield of the pure soluble protein was approximately 40 mg from 1 l culture. A considerable amount of protein was unrecoverable from inclusion bodies. Purified protein eluted from the His-Bind resin in 1 M imidazole buffer was dialyzed extensively against distilled water and lyophilized.

The TEASE ^{13}C-labeled sites are listed in Fig. 1b. Not all carbons were labeled by [2-^{13}C]glycerol due to the specificity of the biosynthetic pathways. The labeled amino acids are mostly hydrophobic residues produced from the glycolysis pathway. Amino acids with polar side chains were produced mostly from the citric acid cycle, and were not labeled due to feedback inhibition. Among the ^{13}C-labeled residues, only valine and leucine have directly bonded ^{13}C pairs. By creating many isolated ^{13}C spins and reducing the number of directly bonded ^{13}C pairs, we reduce the homonuclear ^{13}C–^{13}C dipolar and J-couplings, enhance the spectral resolution, and simplify spectral assignment.

2.2. NMR sample preparation

About 5.5 mg of the soluble colicin sample (without lipids) was transferred into a 4-mm magic-angle spinning (MAS) rotor with a spherical insert. The powder sample was hydrated with deionized and distilled water to a water content of 30 wt.% and sealed.

The membrane-bound colicin was prepared by mixing POPC/POPG lipids with suitable amount of the protein. POPC–d_{31}/POPG (3:1, mol/mol) lipids were mixed in a chloroform solution, which was then evaporated under a stream of nitrogen gas. The resulting lipid film was redissolved in cyclohexane, frozen in liquid nitrogen and freeze-dried under a vacuum of ~50 μbar. Next, 25 mg of the dried lipid powder was hydrated in 1 ml of buffer solution (10 mM KCl, 10 mM citrate, pH 4.8) prepared from doubly deionized water. The lipid suspensions were vortexed and submitted to five freeze–thaw cycles [26] to equilibrate the suspension. Large unilamellar vesicles were prepared by extruding [27] the lipid suspension across polycarbonate filter membranes (five times across a 200 nm filter, and 11 times across a 100 nm filter) using a hand extruder (Avanti Polar Lipids). Aliquots of the extruded lipid vesicles were combined with the appropriate volume of the protein solution to reach a final protein to lipid molar ratio of 1:100. The mixture was then transferred into plastic Ultra-Clear centrifuge tubes and ultracentrifuged at $150\,000 \times g$ for 2 h using a Beckman swinging-bucket rotor (SW60 Ti, Beckman Coulter, Fullerton, CA). The aqueous supernatant was analyzed by a photometric protein assay [28]. The analysis revealed that the supernatant contained only about 5% of the initial concentration of colicin Ia channel domain; thus 95% of the protein has been reconstituted into the lipid membrane. Since the lipid pellet typically contained about 80 wt.% water, the pellet was lyophilized and then rehydrated to a final water content of 30 wt.% and transferred into a 4-mm MAS rotor. The membrane-bound colicin sample contained approximately 8 mg protein and 24 mg lipid.

2.3. NMR spectroscopy

All NMR experiments were carried out on a Bruker DSX-400 spectrometer (Karlsruhe, Germany) operating at a resonance frequency of 400.49 MHz for ^{1}H, 162.12 MHz for ^{31}P, 100.72 MHz for ^{13}C, 40.59 MHz for ^{15}N, and 61.48 MHz for ^{2}H. A triple-resonance MAS probe with a 4-mm spinning module and a double-resonance static probe with a 5-mm solenoid coil were used. The ^{1}H radiofrequency (rf)

field strengths for heteronuclear TPPM decoupling [29] were 80–100 kHz. Carbon and nitrogen 90° pulse lengths were typically 4.0 μs and 5.6 μs, respectively. Cross polarization (CP) contact time was usually 0.7 ms for both the soluble and the membrane-bound sample and 2 ms for the pure lipid sample. Spinning speeds were regulated to ±2 Hz by a pneumatic control unit. A recycle delay of 2–3 s was used. The experiments were carried out either at room temperature ($T = 293 \pm 1$ K) or at 243.0 ± 0.2 K, as measured by the thermocouple in the probe next to the MAS rotor. The low temperature was reached by passing the MAS bearing air through a heat exchanger immersed in liquid nitrogen.

The static lipid ^{31}P spectra were acquired using a single-pulse Hahn-echo sequence. A ^{31}P 90° pulse length of 5 μs, a Hahn-echo delay of 50 μs, a spectral width of 125 kHz, and a recycle delay of 2 s were used. Continuous-wave proton decoupling was applied during signal acquisition.

^{2}H spectra of the *sn*-1 chain-perdeuterated POPC in the presence and absence of colicin Ia channel domain were acquired using a phase-cycled quadrupolar echo pulse sequence [30]. The 3.5-μs ^{2}H 90° pulses were separated by a 50-μs delay. A recycle delay of 0.5 s and a spectral width of 200 kHz were used. The measurements were carried out at 298.0 ± 0.1 K. The ^{2}H powder spectra were dePaked [31] using the algorithm of McCabe and Wassall [32]. Details of the data analysis have been published previously [33]. Briefly, the dePaked spectra were integrated over the peak areas of the methylene groups to derive the order parameter for each carbon along the chain. It is assumed that each methylene group contributes equal intensity to the dePaked spectrum and that the molecular order increases smoothly from the chain terminus to the carbonyl group [34]. The methyl signal of the lipid chain terminus was taken directly from the experimental spectrum since its assignment is definitive. The calculated quadrupolar splittings were converted into order parameters according to $\Delta\nu_Q = 3/4 \times e^2qQ/h \times S(x)$, where $\Delta\nu_Q$ is the measured quadrupolar splitting, e^2qQ/h is the quadrupolar coupling constant, which is 167 kHz for deuterons in C–^{2}H bonds, and $S(x)$ is the chain order parameter for site x in the acyl chains of the phospholipids.

The ^{15}N–^{13}C two-dimensional (2D) heteronuclear correlation (HETCOR) experiment [35,36] and the ^{13}C–^{13}C double-quantum (DQ) INADEQUATE experiment [37] were carried out using published sequences. The ^{13}C rf field strength was seven times the spinning speed for CMR7 dipolar recoupling [38] during the ^{13}C DQ excitation and reconversion periods. One complete cycle of CMR7 (four rotor periods) was used for excitation and reconversion of the double quantum coherence, respectively. The ^{13}C and ^{15}N isotropic chemical shifts were externally referenced to the Gly CO signal at 176.4 ppm (relative to TMS) and the *N*-acetyl-D,L-valine ^{15}N signal at 122 ppm (relative to liquid NH_3).

The ^{13}C chemical shift anisotropy (CSA) was measured by recoupling the CSA interaction using a train of 180° pulses spaced half a rotor period apart (Fig. 2) [39]. The second half of the 180°-pulse train was shifted relative to the first half by a delay τ. The ^{13}C magnetization dephases under the recoupled chemical shift interaction according to the magnitude ($\Delta\sigma$) of CSA and the delay τ. Larger CSAs induce more dephasing. It has been shown that, for β-substituted amino acids, β-sheet conformation has larger Cα CSAs than α-helical structure [40,41]. Thus the amount of dephasing correlates with secondary structure [39]: α-helix signals are less attenuated than β-sheet signals.

The original CSA filter experiment detects single-quantum ^{13}C magnetization. Thus, lipid background ^{13}C signals will appear in the spectrum of the membrane protein sample. This is especially a problem for Val Cβ, which overlaps with the main lipid acyl CH_2 peak. We suppressed the lipid background signals by inserting a ^{13}C double-quantum filter before the 180°-pulse train (Fig. 2). Double-quantum filtration (DQF) was accomplished using a CMR7 homonuclear recoupling sequence [38]. Experiments on [2,3-^{13}C]-labeled Ala confirmed that the simple CSA and DQF-CSA experiments yield identical dephasing curves. Typically, in the DQF-CSA experiment about 25–30% of the intensity is retained compared to the non-DQF CSA filter experiment.

The CSA-filter experiments were carried out at a spinning speed of 5.3 kHz with two rotor periods of CSA recoupling. The ^{15}N decoupling field strength during the CSA evolution period was about 25 kHz. At this spinning speed, the ^{13}C recoupling field strength required for the CMR7 sequence is suffi-

ciently lower than the ^{1}H decoupling field strength, so that a recoupling efficiency of around 50% was achieved.

2.4. Simulations

The CSA time evolution under the 180°-pulse train was simulated using a Fortran program described previously [39]. Sixteen equal intervals of τ were calculated for each CSA magnitude. Powder averaging was carried out at 3° increments for the Euler angles α and β, and 6° steps for the Euler angle γ. The fit parameters are the principal values σ_{ii} ($i = 1, 2, 3$) of the chemical shift tensor, which are related to the CSA span $\Delta\sigma$, asymmetry parameter η, and zero isotropic chemical shift according to $\sigma_{33}-\sigma_{11} = \Delta\sigma$, $(\sigma_{22}-\sigma_{11})/\sigma_{33} = \eta$, $\sigma_{11}+\sigma_{22}+\sigma_{33} = 0$. In all simulations, an asymmetry parameter of $\eta = 0$ was assumed [40].

3. Results

3.1. ^{2}H and ^{31}P NMR spectra of lipids

To verify that the membrane-bound colicin Ia channel domain as prepared above interacts with the lipids, we measured the ^{2}H NMR spectrum of POPC–d_{31}/POPG (Fig. 3) in the absence and presence of the protein. In the absence of the protein, the ^{2}H spectrum shows a maximum quadrupolar splitting of 30.3 kHz (Fig. 3a). This corresponds to a C–^{2}H bond order parameter of 0.24, which is typical for the relatively rigid upper part of the acyl chains. The reduction from the rigid-limit coupling is due to the uniaxial rotational diffusion of the lipid molecules around the bilayer normal. A number of resolved quadrupolar splittings was detected; the smallest among them was 3.1 kHz, which was attributed to the methyl deuterons of the acyl chain terminus.

After colicin Ia channel domain was incorporated into the lipid bilayer, the ^{2}H quadrupolar splittings (Fig. 3b) were significantly reduced for all sites along the chain. The maximum quadrupolar splitting decreased to 25.5 kHz ($S_{CD} = 0.20$) and the methyl groups showed a splitting of only 2.1 kHz. Moreover, the spectral resolution deteriorated, manifested by the disappearance of the sharp edges of the peaks. This suggests intermediate-timescale motions of the lipids induced by colicin Ia. The changes of the ^{2}H quadrupolar splittings confirm that, under the sample preparation protocol used here, colicin Ia channel domain interacts with the lipid bilayer on a molecular length scale rather than forming separate domains.

To further illustrate the large increase of lipid bilayer disorder due to colicin binding, we converted the ^{2}H quadrupolar splittings to order parameters (S_{CD}) for individual deuterons along the acyl chains using the dePaking procedure. Smoothed order parameters were calculated from the integrated intensity of the dePaked spectrum [31,33,34]. These ^{2}H order parameters and quadrupolar couplings were plotted as a function of the acyl chain position in Fig. 3d. A characteristic profile of decreasing order

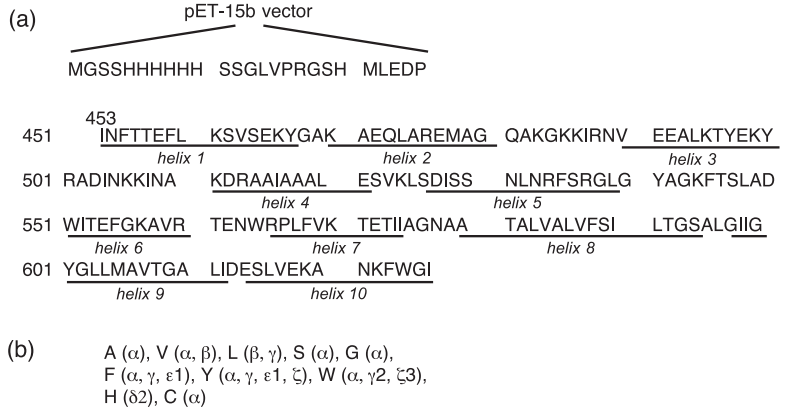

Fig. 1. (a) Amino acid sequence of the colicin Ia channel domain studied here. (b) ^{13}C-Labeled sites by the [2-^{13}C]glycerol TEASE labeling scheme [24].

parameters with increasing distance from the glycerol backbone was obtained [42,43] both for the pure bilayer and for the colicin-bound bilayer. But the latter showed reduced order parameters throughout (Fig. 3d).

To assess how well the dePaking procedure reproduces the experimental spectrum, given the increased linewidths of the protein–lipid mixture, we simulated a ^{2}H spectrum using the order parameters for the colicin-bound lipids (Fig. 3c). The simulated spectrum containing a superposition of fifteen Pake doublets shows satisfactory agreement with the experimental spectrum (Fig. 3b), indicating that the order parameter profile adequately describes the colicin–lipid mixture. On average, the lipid ^{2}H quadrupolar splittings were reduced by 23% upon colicin binding, which represents a decrease in lipid chain length of 0.8 Å. This can be converted to an increase in lipid area per molecule, since chain order determines cross-sectional area of each lipid molecule [44]. We found an increase in area per lipid molecule of 4.4 Å^2 due to the binding of colicin Ia channel domain to the lipid bilayer. A similar reduction of lipid chain order was also observed for colicin A [45].

The static ^{31}P NMR spectra of the phospholipids with and without colicin Ia channel domain are shown in Fig. 4. The spectra consist of a superposition of two axially symmetric powder spectra. From the PC/PG ratio one can conclude that the spectrum with the smaller CSA represents the PG and the spectrum with the larger CSA is due to PC. The spectra in the presence and absence of colicin showed similar powder lineshapes, both with $\eta = 0$. This indicates that the lipid bilayers remain in the liquid-crystalline Lα phase after colicin binding, and do not form isotropic or inverse hexagonal phases with high

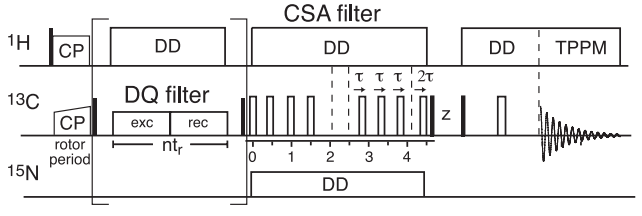

Fig. 2. Pulse sequence for measuring the chemical shift anisotropy of colicin Ia channel domain. An optional double-quantum filter is applied before the CSA filter to select ^{13}C–^{13}C spin pairs. Filled and open rectangles represent 90° and 180° pulses, respectively. DD, dipolar decoupling.

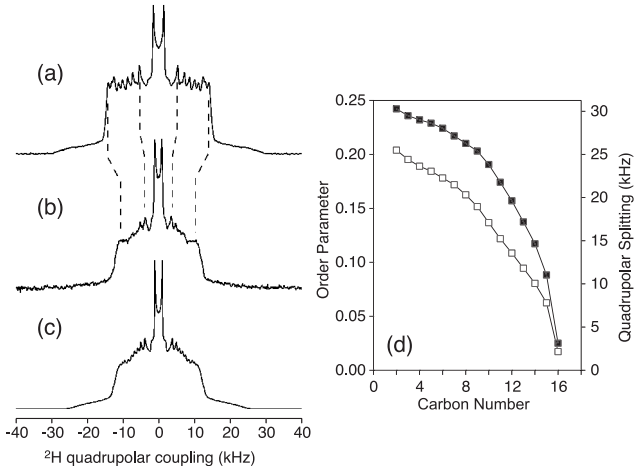

Fig. 3. Static ^{2}H spectra of POPC–d_{31}/POPG lipids in the absence (a) and presence (b) of colicin. (c) Numerical simulation of spectrum b using 15 Pake doublets with quadrupolar splittings calculated from the lower order parameter profile in d. Different exponential line broadening was applied for various peaks of the simulated spectrum: 100 Hz for the methyl signal (C16), 300 Hz for C15 and C14, 450 Hz for C13 and C12, and 500 Hz for C11–C2. (d) ^{2}H order parameters after dePaking. Filled symbols, pure lipids; open symbols, colicin-bound lipids. Number of scans (NS): 6400 for spectrum a (~10 mg total lipids) and 17 880 for spectrum b (1.5 mg colicin in 4.5 mg lipids). The POPC/POPE molar ratio was 3:1, and the colicin/lipid molar ratio was 1:100.

curvatures. Thus, the reduced ^{2}H quadrupolar splittings do not result from protein-induced membrane curvature. After colicin binding, the lipid ^{31}P spectrum shows increased intrinsic linewidth (decreased T_2), suggesting slower motions of the lipid molecules. A somewhat smaller ^{31}P CSA is detected for the membrane-bound sample, as seen from lineshape simulations in Fig. 4c,d. This supports our ^{2}H results and indicates that colicin Ia channel domain interacts with the lipid headgroups.

3.2. ^{13}C isotropic chemical shifts of colicin Ia channel domain

To compare the conformations of the two states of colicin Ia channel domain, we examined the isotropic chemical shift spectra of the soluble and the membrane-bound protein under MAS. Isotropic chemical shifts of proteins reflect the backbone conformation [46–49]. For example, the Cα chemical shifts in helix and sheet residues are displaced by as much as 4 ppm from the random coil frequency downfield and up-

field, respectively (helix: 65.3 ppm; sheet: 60.0 ppm; random coil: 62.3 ppm) [49]. Other effects such as hydrogen bonding and side chain geometry cause smaller chemical shift changes, mainly to the ^{15}N and ^{13}CO spins [50]. Thus, the isotropic chemical shifts should shed light on secondary structural differences between the two forms of colicin Ia channel domain.

Fig. 5a shows ^{1}H-decoupled ^{13}C MAS spectrum of the soluble colicin Ia channel domain at a temperature of 20°C. The Cα region shows a number of resolved peaks with linewidths of 1.2–1.5 ppm. Tentative assignments, based on the ^{13}C labeling scheme and the characteristic chemical shifts [51] of amino acids, are given in the figure. The assignments for Val, Gly, and Leu sites are confirmed by 2D correlation experiments shown below.

In comparison, the spectrum of the membrane-bound colicin, also acquired at room temperature, shows a noticeable redistribution of spectral intensity (Fig. 5b). Most prominently, the intensities around 57 ppm decreased while the 59.6-ppm peak increased in intensity, creating a valley-like region in the spectrum. The resolution of the membrane-protein spectrum is reduced compared to the soluble sample,

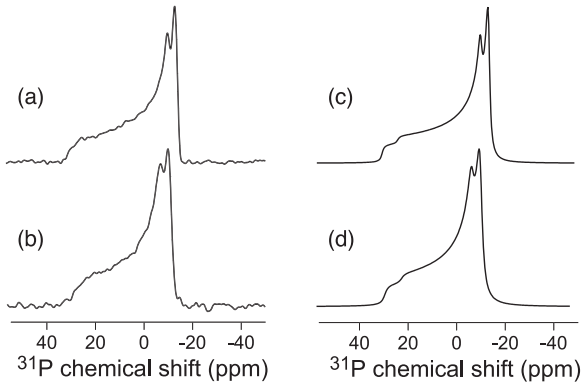

Fig. 4. ^{31}P spectra of static POPC–d_{31}/POPG bilayers without (a) and with (b) colicin Ia channel domain. The spectra consist of a superposition of two axially symmetric powder patterns for POPC and POPG, respectively. From the intensities of the upfield peaks of the spectra and the 1:3 molar ratio of PC and PG lipids, it is concluded that the smaller powder pattern corresponds to POPG and the larger powder pattern to POPC. Simulated ^{31}P NMR spectra are shown in the absence (c) and presence (d) of colicin Ia channel domain. Spectra were simulated by the superposition of two axially symmetric tensors with $\Delta\sigma_1 = 44.3$ ppm and $\Delta\sigma_2 = 34.5$ ppm for c, and $\Delta\sigma_1 = 39.8$ ppm and $\Delta\sigma_2 = 29.3$ ppm for d, at a 3:1 intensity ratio.

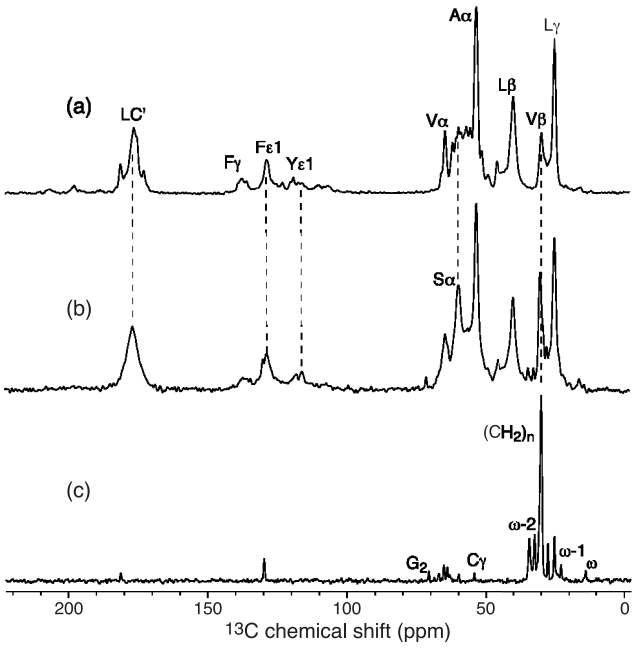

Fig. 5. ^{13}C CP-MAS spectra of the (a) soluble and (b) membrane-bound colicin Ia channel domain. NS = 1024 for each spectrum. (c) ^{13}C spectrum of pure POPC:POPG. NS = 4392. All spectra were acquired at room temperature (20°C). CP contact time was 0.7 ms for the colicin samples and 2 ms for the lipid. Spinning speed: 7 kHz.

analogous to the ^{2}H and ^{31}P spectra. A number of additional weak and sharp signals were observed that can be attributed to the lipid ^{13}C signals at natural abundance. This is verified by the ^{13}C CP spectrum of a pure POPC–d_{31}/POPG sample in the liquid-crystalline phase state at 20°C (Fig. 5c) [52]. In the following experiments, these lipid background signals were removed either by passing through the ^{15}N coherence or by a ^{13}C–^{13}C double-quantum filter.

A representative ^{13}C–^{13}C DQ spectrum of the membrane-bound colicin at $T = 243$ K is shown in Fig. 6a. At the short coherence transfer time of four rotor periods (0.57 and 0.67 ms for 7 and 6 kHz spinning speed, respectively) used, the experiment detects only the directly bonded ^{13}C spin pairs [37,53]. The [2-^{13}C]glycerol TEASE ^{13}C-labeling scheme provides two pairs of directly bonded ^{13}C sites, Val Cα–Cβ and Leu Cβ–Cγ. Thus, the ^{13}C DQF spectrum is greatly simplified compared to the CP spectrum, and all four peaks are assigned unambiguously. The identification of the Val Cα (65.0 ppm) and Cβ (29.6 ppm) peaks allow their chemical shift analysis, as shown below.

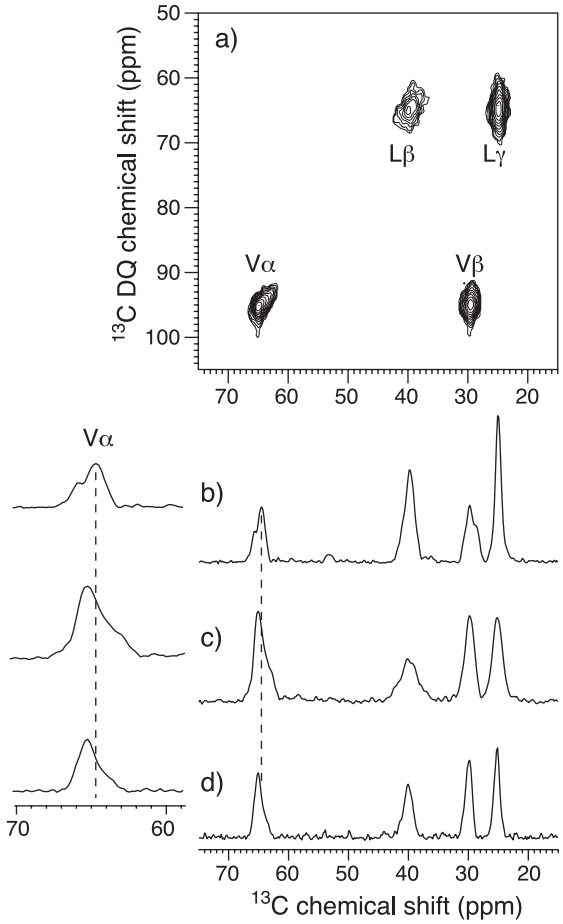

Fig. 6. ^{13}C DQ spectra of colicin, acquired at 7 kHz for soluble and 6 kHz for membrane-bound sample. (a) 2D DQ spectrum of membrane-bound colicin at 243 K. NS per t_1 slice: 224. (b) Projection of the 2D spectrum of soluble colicin onto the single-quantum dimension. NS per t_1 slice: 288. (c) Projection of the 2D spectrum of membrane protein (shown in a) at 243 K. On the left-hand side, the Val Cα signals have been expanded. Dashed vertical line guides the eye for the different isotropic shifts of the Val Cα. (d) Projection of the 2D spectrum of membrane-bound colicin at 293 K. NS per t_1 slice: 192.

The 2D DQ spectra of the two states of colicin show small isotropic shift differences, which are best examined by comparing the 1D projections of the 2D spectra onto the directly detected dimension (Fig. 6b,c). It can be seen that the maximum of the Val Cα signal is shifted downfield by 0.6 ppm in the membrane-bound state (see extended Cα region on the left hand side of Fig. 6), From the peak shape it can be rationalized that some of the Val Cα signals have shifted downfield. This small downfield shift persists even when the membrane protein was at room temperature (Fig. 6d), indicating that the conformation of the Val residues are not significantly altered by lipid motions. The low temperature does induce larger linewidths, indicating faster relaxation of the immobilized protein.

The ^{13}Cα isotropic chemical shifts were further resolved by 2D ^{15}N–^{13}C correlation spectra (Fig. 7). Several type assignments are made, although detailed analysis and sequence-specific assignment are not possible at this time due to the lack of complete site resolution. In the soluble protein spectrum (Fig. 7a), the most downfield ^{13}Cα peaks at around 65 ppm can be unambiguously assigned to Val residues based on the DQ spectra. The amide ^{15}N chemical shifts of these Val residues helped resolve many of these Val peaks. In comparison, the spectrum of the membrane-bound colicin (Fig. 7b) shows clear intensity redistribution and peak shifts. For example, a

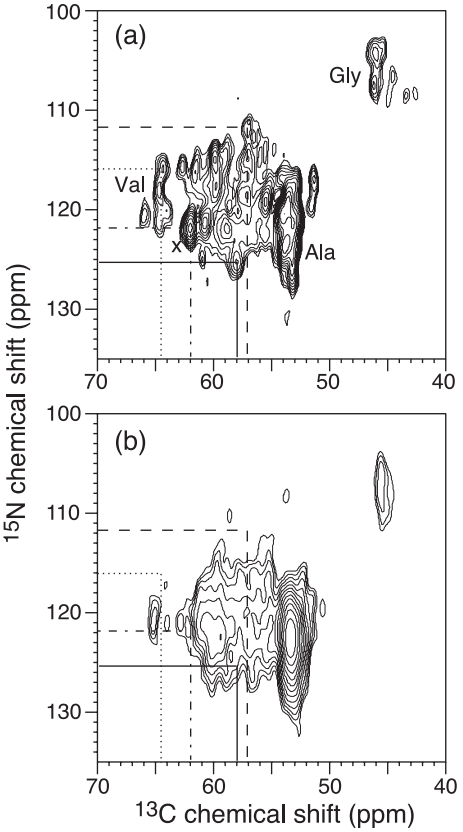

Fig. 7. ^{15}N–^{13}C 2D correlation spectra of the soluble (a) and membrane-bound (b) colicin Ia channel domain, acquired at 293 K for (a) and 243 K for (b). NS per t_1 slice: 576 for (a) and 416 for (b). Spinning speed: 7 kHz for (a) and 6 kHz for (b). Lines guide the eye for differences between the two spectra.

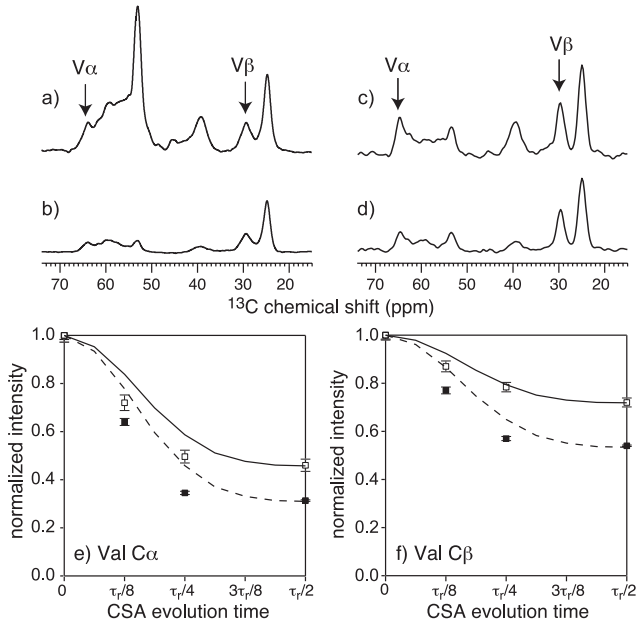

Fig. 8. CSA filter spectra of soluble (a,b) and membrane-bound (c,d) colicin. Spectra (c,d) were acquired with DQF to suppress the lipid signals. CSA evolution times: $\tau = 0$ for a,c and $\tau = \tau_r/2$ for b,d. Arrows indicate the Val Cα and Cβ signals for which CSA evolution was analyzed below. Spectra were acquired with 2048 (a), 8192 (b), 5120 (c), and 12 800 (d) scans at 243 K and 5.3 kHz spinning. (e) Val Cα CSA dephasing curves. (f) Val Cβ CSA dephasing curves. Weaker dephasing is observed for the membrane protein (open symbols) than for the soluble colicin (filled symbols). Dashed (solid) lines: simulated CSA decay curves for the soluble (membrane-bound) colicin.

strong peak at (62 ppm, 122 ppm) (marked by X) in the soluble spectrum became unresolved in the membrane sample spectrum. The Val cluster showed a small downfield shift, consistent with the DQF spectra. Overall, the membrane protein spectrum is broadened in both the ^{13}C and ^{15}N dimensions compared to the soluble colicin spectrum.

3.3. ^{13}C anisotropic chemical shifts of colicin Ia channel domain

Fig. 8a–d shows the aliphatic region of the CSA filter spectra of the soluble and membrane-bound colicin Ia channel domain. CSA evolution times of zero (top row) and half a rotor period (bottom row) are shown. DQ filtration was applied to the membrane protein sample to remove the lipid background signals. All spectra were acquired at 243 K to freeze out motions and obtain the rigid-limit CSAs. Quantitative decay curves for the resolved and assigned Val Cα and Cβ signals are shown in Fig. 8e,f. Both Cα and Cβ sites exhibit reduced CSAs in the membrane-bound state than the soluble state. Based on the intensities at the half rotor period, the Val Cα CSA span is 21 ± 1 ppm in the membrane-bound state and 25 ± 1 ppm in the soluble state (Table 1). The Val Cβ CSA span is 14 ± 1 ppm for the membrane sample and 19 ± 1 ppm for the soluble protein. These values fall into the general range expected for the α-helical conformation, as predicted by quantum chemical calculations [40]. Depending on the χ_1 angle, these calculations have found Val Cα $\Delta\sigma$ values of 32–37 ppm for β sheet and 15–29 ppm for α helix.

We have also measured the CSA values for soluble and membrane-bound colicin at room temperature (see Table 1). Due to molecular motions at room temperature, the CSA tensors are scaled and need to be corrected to obtain the full CSA value. In a previous study, we have measured the segmental order parameters for all resolved signals of colicin [24]. The full span of the CSA tensor is obtained by dividing the room-temperature values by these order parameters. Similar to the results at low temperature, the CSA value for the Val residues increases upon membrane binding. In other words, the CSA gap between the two forms of the protein persists at both room temperature and low temperature, with the membrane-bound colicin having smaller CSAs.

Table 1
Comparison of the ^{13}C CSA spans ($\Delta\sigma$) for Val Cα and Cβ of the soluble and the membrane-bound (MB) states of colicin Ia channel domain

Peaks	Temperature (K)	$\Delta\sigma$ (ppm)[a]		$\Delta(\Delta\sigma)$ (ppm)
		Soluble	MB[b]	$\Delta\sigma$(MB)−$\Delta\sigma$(sol)
Val Cα	243	25 ± 1	21 ± 1	−4
Val Cβ	243	19 ± 1	14 ± 1	−5
Val Cα	293	23 ± 1[c]	21 ± 1[c]	−2
Val Cβ	293	18 ± 1[c]	16 ± 1[c]	−2

[a]$\Delta\sigma$ determined from the best fit of experimental data to simulations of CSA dephasing curves calculated with an asymmetry parameter of $\eta = 0$.
[b]Obtained from the DQF-CSA experiment.
[c]Values were corrected for mobility using the order parameters for Val Cα and Cβ obtained from C–H dipolar coupling measurements (soluble colicin: $S_{C\alpha} = 1.00$, $S_{C\beta} = 0.88$; membrane bound colicin: $S_{C\alpha} = 0.90$, $S_{C\beta} = 0.75$) [24].

The experimental decay intensities at $\tau_r/8$ and $\tau_r/4$ are lower than in the simulated curves. This may result from the Cα–Cβ dipolar couplings, which are not fully compensated by the CSA filter sequence except for evolution times of $\tau = 0$, $\tau_r/2$, and τ_r. The effect of the homonuclear coupling is strongest at $\tau = \tau_r/4$. Therefore, simulations were optimized to fit the data at $\tau_r/2$. Nevertheless, this imperfection does not affect the empirical observation that the membrane-bound colicin has smaller CSAs than the soluble colicin, since the one-bond ^{13}C–^{13}C homonuclear coupling is identical for the two samples at this low temperature.

We also measured the ^{13}C CSAs at room temperature (293 K) for both samples (Table 1) to probe the biologically relevant state of the protein. To take into account the effect of motion, we scaled up the CSA values by the inverse of the C–H order parameters for the corresponding sites obtained from separate experiments [24]. These mobility-corrected CSA values agreed well with the low-temperature results for the membrane protein (Table 1).

4. Discussion

Colicin Ia channel domain is particularly amenable to solid-state NMR studies. It is soluble in water, and reconstitution of the protein into lipid bilayers is straightforward since the molecule inserts spontaneously into membranes. When preparing the membrane protein sample, we first mixed colicin with unilamellar lipid vesicles to maximize the protein–lipid interaction. Then the amount of water was reduced to make the sample suitable for solid-state NMR. Thus, the colicin-containing bilayers were finally arranged in membrane stacks (multilamellar vesicles) at a lower hydration level. However, this lower hydration level is still sufficient for this membrane protein, as supported by our recent investigation of the dynamics of membrane-bound colicin [24]. In that study, we showed that colicin Ia channel domain is much more mobile than other membrane proteins of similar or even smaller molecular masses. Therefore, the somewhat restricted water space between bilayers should not compromise the study of conformational changes of membrane-bound colicin Ia channel domain.

The measured ^{13}C isotropic chemical shifts of colicin Ia channel domain indicate that the secondary structure of the protein, to first order, is similar and highly helical in the soluble and the membrane-bound states. The Val Cα and Cβ isotropic shifts, which are resolved and definitively assigned, are broadly consistent with those expected for the helical conformation. The persistence of the helical structure after membrane binding is not surprising, since the soluble state of colicin Ia channel domain is already 78% helical [4], and membrane binding, while known to promote helix formation, is unlikely to increase the helical content much further.

Despite this overall similarity, careful examination shows that the Val Cα isotropic shift increased by 0.6 ppm upon membrane binding. Corroborating this result we have measured a decrease in Val Cα and Cb CSA. These results suggest an ordering of the helical structure due to membrane binding. While most (eight out of nine) Val residues reside in helices in the soluble protein, not all these residues adopt ideal helical torsion angles according to the crystal structure. The residues located at the edges of the helices such as V490 ($\phi = -46°$, $\psi = -69°$) and V559 ($\phi = -73°$, $\psi = -21°$) have torsion angles that deviate significantly from those of ideal α-helices ($\phi = -57°$, $\psi = -47°$). Based on the statistical analysis of protein chemical shifts from empirical databases [50], these torsion angles would yield a downfield shift of 2–2.5 ppm from the random coil values. This is smaller than the isotropic shifts expected for six other Val residues (V463, V569, V584, V587, V607 and V617) that have more ideal helical torsion angles (about 3 ppm). In other words, the Val Cα sites in the soluble state of colicin would have less than maximal secondary shifts due to slight distortions of the helical structure. These distortions may result from interhelical loops and tertiary contacts in the compact protein. As the protein spreads out onto the membrane surface, however, the distorted helices may become more ordered and closer to ideal, thus the Val Cα sites exhibit more downfield-shifted isotropic peaks.

The ^{15}N–^{13}C 2D spectra are consistent with the conclusions from the ^{13}C chemical shifts. It can be appreciated, even without full assignment, that the two conformations of the proteins yield spectra with the same overall frequency ranges, but with different intensity distributions. Thus, large changes of

the helical content are unlikely, but the helices existing in the soluble form may be refined due to membrane binding.

The hypothesis of helix ordering is consistent with a recent fluorescence study of colicin E1 channel domain [16,54], which shows that the protein forms an extended helical array on the membrane surface, a very different tertiary structure from its soluble state. In this model, the densely packed colicin channel domain in solution becomes much more open and flexible upon membrane binding: the helices drift apart, and eventually occupy a large area, about 4200 Å^2 for colicin E1, in the membrane [16,54]. This extended helical array model is also consistent with the reduced ^{2}H quadrupolar couplings of the colicin-bound lipids: if colicin Ia channel domain predominantly binds at the lipid–water interface, then it should cause lateral expansion of the bilayer and permit increased motional freedom in the acyl chains. Through the partial unfolding of the tertiary structure of membrane-bound colicin Ia channel domain, more lipid molecules interact with the protein and become disordered. The degree of observed ^{2}H order parameter reduction also appears to be indicative of an extended colicin at the bilayer–water interface. This is inferred from comparison with a previous study of a 21-residue surface-bound single-helix peptide, which shows a similar amount of ^{2}H order parameter reduction [55]. In that study, the peptide/lipid molar ratio was 1:10, compared to the molar ratio of 1:100 used here. However, if all ten helices in colicin Ia channel domain become exposed to the lipids due to the partial unfolding and extension, then the effective helix/lipid molar ratio becomes comparable to that of the previous study. In other words, the similar mass concentration of the surface-bound peptide in both studies induces a similar increase in the lipid chain disorder.

The reduced Val Cα and Cβ CSAs are consistent with the isotropic chemical shift data in supporting our conclusion that membrane binding makes the helices more ordered and ideal. The somewhat larger changes in the CSA span than the isotropic shift are possible, since quantum chemical calculations have shown that the outer two principal values of the chemical shift tensor can move in opposite directions, thus changing the anisotropic span but not the isotropic shift. For example, the Val Cα isotropic shielding differs by 5–7 ppm between sheet and helix, but its CSA span changes by 8–22 ppm, depending on the side chain torsion angle, χ_1 [40].

5. Conclusion

We have measured the ^{13}C isotropic and anisotropic chemical shifts of the water-soluble and membrane-bound states of colicin Ia channel domain, and the effect of colicin binding on lipid bilayers by ^{2}H and ^{31}P NMR. The Val ^{13}Cα and ^{13}Cβ isotropic shifts are only moderately different between the two states, indicating that the helical content of the protein is overall comparable between the two states, in agreement with optical measurements [17]. The small isotropic chemical shift increase (0.6 ppm) and the 4-ppm anisotropic chemical shift decrease of Val Cα in the membrane-bound colicin compared to the soluble state suggest that the helices become more ideal and ordered upon membrane binding. This happens if colicin Ia channel domain extends itself onto the membrane surface, forming an open tertiary structure, in contrast to the compact globular shape of the soluble protein. Colicin binding significantly increases the lipid chain disorder, as manifested by the reduced ^{2}H quadrupolar couplings of the perdeuterated POPC chains. This increased bilayer disorder is also consistent with a model of a loosely packed colicin Ia channel domain predominantly associated with the bilayer surface [16,54]. Our results would be in agreement both with the umbrella and the penknife model of membrane bound colicin if the arrangement in an extended helical array is incorporated into these models. The distinction between these two models can be made by ^{1}H spin diffusion experiments, which are presented elsewhere [56].

Acknowledgements

M.H. thanks the Arnold and Mabel Beckman Foundation for a Young Investigator Award, the National Science Foundation for a CAREER award (MCB-0093398), and Research Corporation for a Research Innovation Award. D.H. is grateful for a postdoctoral fellowship from the BASF AG and the Studienstiftung des deutschen Volkes.

References

[1] R. Stroud, Curr. Opin. Struct. Biol. 5 (1995) 514–520.
[2] W.A. Cramer, J.B. Heymann, S.L. Schendel, B.N. Deriy, F.S. Cohen, P.A. Elkins, C.V. Stauffacher, Annu. Rev. Biophys. Biomol. Struct. 24 (1995) 611–641.
[3] H. Zhan, K.J. Oh, Y.-K. Shin, W.L. Hubbell, R.J. Collier, Biochemistry 34 (1995) 4856–4863.
[4] M. Wiener, D. Freymann, P. Ghosh, R.M. Stroud, Nature 385 (1997) 461–464.
[5] M.W. Parker, J.P.M. Postma, F. Pattus, A.D. Tucker, D. Tsernoglou, J. Mol. Biol. 224 (1992) 639–657.
[6] P. Elkins, A. Bunker, W.A. Cramer, C.V. Stauffacher, Structure 5 (1997) 443–458.
[7] I.R. Vetter, M.W. Parker, A.D. Tucker, J.H. Lakey, F. Pattus, D. Tsernoglou, Structure 6 (1998) 863–874.
[8] J.A. Mankovich, C.H. Hsu, J. Konisky, J. Bacteriol. 168 (1986) 228–236.
[9] J.B. Heymann, S.D. Zakharov, Y.L. Zhang, W.A. Cramer, Biochemistry 35 (1996) 2717–2725.
[10] D. Massotte, M. Yamamoto, S. Scianimanico, O. Sorokine, A.v. Dorsselaer, Y. Nakatani, G. Ourisson, F. Pattus, Biochemistry 32 (1993) 13787–13794.
[11] Y. Kim, K. Valentine, S.J. Opella, S.L. Schendel, W.A. Cramer, Protein Sci. 7 (1998) 342–348.
[12] S. Lambotte, P. Jasperse, B. Bechinger, Biochemistry 37 (1998) 16–22.
[13] J.H. Lakey, D. Duche, J. Gonzalez-Manas, D. Baty, F. Pattus, J. Mol. Biol. 230 (1993) 1055–1067.
[14] K.K. Kumashiro, K. Schmidt-Rohr, O.J. Murphy, K.L. Ouellette, W.A. Cramer, L.K. Thompson, J. Am. Chem. Soc. 120 (1998) 5043–5051.
[15] E. Goormaghtigh, L. Vigneron, M. Knibiehler, C. Lazdunski, J.M. Ruysschaert, Eur. J. Biochem. 202 (1991) 1299–1305.
[16] S.D. Zakharov, M. Lindeberg, Y. Griko, Z. Salamon, G. Tollin, F.G. Prendergast, W.A. Cramer, Proc. Natl. Acad. Sci. USA 95 (1998) 4282–4287.
[17] S.F. Mel, R.M. Stroud, Biochemistry 32 (1993) 2082–2089.
[18] P. Rath, O. Bousche, A.R. Merrill, W.A. Cramer, K.J. Rothschild, Biophys. J. 59 (1991) 516–522.
[19] H. Suga, K. Shirabe, T. Yamamoto, M. Tasumi, M. Umeda, C. Nishimura, A. Nakazawa, M. Nakanishi, Y. Arata, J. Biol. Chem. 266 (1991) 13537–13543.
[20] F.G. van der Goot, J.M. Gonzalex-Manas, J.H. Lakey, F. Pattus, Nature 354 (1991) 408–410.
[21] S.O. Smith, K. Aschheim, M. Groesbeek, Q. Rev. Biophys. 29 (1996) 395–449.
[22] R. Fu, T.A. Cross, Annu. Rev. Biophys. Biomol. Struct. 28 (1999) 235–268.
[23] F. Marassi, S. Opella, Curr. Opin. Struct. Biol. 8 (1998) 640–648.
[24] D. Huster, L.S. Xiao, M. Hong, Biochemistry 40 (2001) 7662–7674.
[25] M. Hong, K. Jakes, J. Biomol. NMR 14 (1999) 71–74.
[26] L.D. Mayer, M.J. Hope, P.R. Cullis, A.S. Janoff, Biochim. Biophys. Acta 817 (1985) 193–196.
[27] M.J. Hope, M.B. Bally, G. Webb, P.R. Cullis, Biochim. Biophys. Acta 812 (1985) 55–65.
[28] P.K. Smith, R.I. Krohn, G.T. Hermanson, A.K. Mallia, F.H. Gartner, M.D. Provenzano, E.K. Fujimoto, N.M. Goeke, B.J. Olson, D.C. Klenk, Anal. Biochem. 150 (1985) 76–85.
[29] A.E. Bennett, C.M. Rienstra, M. Auger, K.V. Lakshmi, R.G. Griffin, J. Chem. Phys. 103 (1995) 6951–6958.
[30] J.H. Davis, K.R. Jeffrey, M. Bloom, M.I. Valic, T.P. Higgs, Chem. Phys. Lett. 42 (1976) 390–394.
[31] E. Sternin, M. Bloom, L. MacKay, J. Magn. Reson. 55 (1983) 274–282.
[32] M.A. McCabe, S.R. Wassall, J. Magn. Reson. B 106 (1995) 80–82.
[33] D. Huster, K. Arnold, K. Gawrisch, Biochemistry 37 (1998) 17299–17308.
[34] M. Lafleur, B. Fine, E. Sternin, P.R. Cullis, M. Bloom, Biophys. J. 56 (1989) 1037–1041.
[35] C.A. Michal, L.W. Jelinski, J. Am. Chem. Soc. 119 (1997) 9059–9060.
[36] M. Hong, R.G. Griffin, J. Am. Chem. Soc. 120 (1998) 7113–7114.
[37] M. Hong, J. Magn. Reson. 136 (1999) 86–91.
[38] C.M. Rienstra, M.E. Hatcher, L.J. Mueller, B.Q. Sun, S.W. Fesik, R.G. Griffin, J. Am. Chem. Soc. 120 (1998) 10602–10612.
[39] M. Hong, J. Am. Chem. Soc. 122 (2000) 3762–3770.
[40] R.H. Havlin, H. Le, D.D. Laws, A.C. deDios, E. Oldfield, J. Am. Chem. Soc. 119 (1997) 11951–11958.
[41] N. Tjandra, A. Bax, J. Am. Chem. Soc. 119 (1997) 9576–9577.
[42] A. Seelig, J. Seelig, Biochemistry 13 (1974) 4839.
[43] J. Seelig, A. Seelig, Q. Rev. Biophys. 13 (1980) 19–61.
[44] J.F. Nagel, Biophys. J. 64 (1993) 1476–1481.
[45] V. Geli, M.C. Koorengevel, R.A. Demel, C. Lazdunski, J.A. Killian, Biochemistry 31 (1992) 11089–11094.
[46] S. Spera, A. Bax, J. Am. Chem. Soc. 113 (1991) 5490–5492.
[47] D.S. Wishart, B.D. Sykes, F.M. Richards, J. Mol. Biol. 222 (1991) 311–333.
[48] H. Saito, Magn. Reson. Chem. 24 (1986) 835–852.
[49] D.S. Wishart, B.D. Sykes, Methods Enzymol. 239 (1994) 363–392.
[50] M. Iwadate, T. Asakura, M.P. Williamson, J. Biomol. NMR 13 (1999) 199–211.
[51] J.N.S. Evans, Biomolecular NMR Spectroscopy, Oxford University Press, Oxford, 1995.
[52] J. Forbes, C. Husted, E. Oldfield, J. Am. Chem. Soc. 110 (1988) 1059–1065.
[53] A. Bax, R. Freeman, S.P. Kempsell, J. Am. Chem. Soc. 102 (1980) 4849–4851.
[54] M. Lindeberg, S.D. Zakharov, W.A. Cramer, J. Mol. Biol. 295 (2000) 679–692.
[55] B.W. Koenig, J.A. Ferretti, K. Gawrisch, Biochemistry 38 (1999) 6327–6334.
[56] D. Huster, X.L. Yao, M. Hong, J. Am. Chem. Soc. 124 (2002) 874–883.